

Single-crystal sum-frequency-generating optical parametric oscillator

Kahraman G. Köprülü, Tolga Kartaloğlu, Yamaç Dikmelik, and Orhan Aytür

Department of Electrical and Electronics Engineering, Bilkent University, TR-06533 Bilkent, Ankara, Turkey

Received August 11, 1998; revised manuscript received December 17, 1998

We report a synchronously pumped optical parametric oscillator that generates the sum frequency of the pump and the signal wavelengths. A single KTiOPO_4 (KTP) crystal is used for both parametric generation and sum-frequency generation in which these two processes are simultaneously phase matched for the same direction of propagation. The parametric oscillator, pumped by a femtosecond Ti:sapphire laser at a wavelength of 827 nm, generates a blue output beam at 487 nm with 43% power-conversion efficiency. The polarization geometry of simultaneous phase matching requires rotation of the pump polarization before the cavity. Adjusting the group delay between the two orthogonally polarized pump components to compensate for the group-velocity mismatch in the KTP crystal increases the photon-conversion efficiency more than threefold. Angle tuning in conjunction with pump wavelength tuning provides output tunability in the 484–512-nm range. A plane-wave model that takes group-velocity mismatch into account is in good agreement with our experimental results. © 1999 Optical Society of America [S0740-3224(99)01309-0]

OCIS codes: 190.2620, 190.4410, 190.4970, 190.7110, 190.7220.

1. INTRODUCTION

Optical parametric oscillators (OPO's) are widely used for tunable wavelength conversion of lasers to previously unavailable wavelength ranges.¹ An OPO downconverts a higher-frequency pump beam into lower-frequency signal and idler beams through parametric generation in a second-order nonlinear material. The signal and idler frequencies are determined by the phase-matching condition in the nonlinear crystal. This condition is usually satisfied by either birefringent phase matching,² in which the natural birefringence of the crystal is utilized, or quasi-phase matching,³ in which periodic domain reversals fabricated into the crystal lead to a grating momentum that cancels the natural phase mismatch. Modifying the phase-matching condition by changing the angle, the temperature, or the quasi-phase-matching period brings tunability to OPO's, making them versatile sources of laser radiation.

By itself, an OPO can provide only downconversion to longer wavelengths. Several researchers⁴ have demonstrated the utility of synchronously pumped OPO in the ultrafast regime as sources of tunable infrared radiation.⁵ However, upconversion to shorter wavelengths requires the use of second-harmonic generation or sum-frequency generation (SFG) in conjunction with an OPO. One approach is to frequency double the pump laser and use the second harmonic as the OPO pump.⁶ A more widely used technique is to frequency double the signal (or the idler) beam outside⁷ or inside⁸ the OPO cavity. Intracavity second-harmonic generation is usually preferred because with it one can take advantage of the high intensity of the resonant field. SFG of the signal or the idler with the residual (unconverted) pump also provides upconversion and can be implemented extracavity or intracavity.^{9,10} These upconversion OPO's have successfully generated tunable ultrafast pulses at visible wavelengths, mostly, however, with limited conversion efficiencies (~10%), ex-

cept for those found in the research reported in Ref. 10 (25% efficiency with SFG, 31% with second-harmonic generation).

In this paper we report a synchronously pumped single-crystal sum-frequency-generating OPO (SF-OPO) for which the SFG process takes place within the OPO crystal itself.¹¹ The SF-OPO is based on the premise that both optical parametric generation and SFG can be phase matched for the same direction of propagation inside the same nonlinear crystal.¹² In principle, this simultaneous phase-matching condition can be achieved with either birefringent phase matching or quasi-phase matching. Our SF-OPO is based on a KTiOPO_4 (KTP) crystal, for which birefringent phase matching is used for both processes. The polarization geometry of the two phase-matching conditions necessitates a pump polarization that is at an angle to the fast and slow axes of the birefringent KTP crystal. Adjusting the group delay between the fast and the slow components of the pump to compensate for the group-velocity mismatch in the KTP crystal increases the photon-conversion efficiency more than threefold. We have demonstrated 43% power-conversion efficiency (50% photon-conversion efficiency) from the pump to the sum-frequency beam.

The phase-matching geometry and the experimental setup are described in Section 2. Experimental measurements and results, including conversion efficiency, tuning range, and pulse characteristics, are discussed in Section 3. A plane-wave model of pulse propagation in the SF-OPO is outlined in Section 4. Finally, Section 5 summarizes our results and conclusions.

2. EXPERIMENTAL SETUP

A. Phase Matching

Our experiments are based on simultaneous phase matching of the parametric generation and SFG processes

in a KTP crystal that is pumped by a Ti:sapphire laser. The KTP crystal is cut for noncritical phase matching with $\theta = 90^\circ$ and $\phi = 0^\circ$. When it is pumped at a wavelength of 827 nm, the KTP crystal is phase matched for parametric generation with signal and idler wavelengths of 1182 and 2756 nm, respectively. In this type III phase-matching geometry the pump and the signal beams are polarized along the fast axis and the idler beam is polarized along the slow axis of the birefringent KTP crystal. For the same direction of propagation, the KTP crystal is also phase matched for SFG of the signal and the pump wavelengths in a type II polarization geometry. Here, the higher-frequency SFG input at the pump wavelength is polarized along the slow axis and the lower-frequency SFG input at the signal wavelength is polarized along the fast axis. Inasmuch as the polarizations of the OPO pump and of the higher-frequency SFG input are orthogonal, rotation of the laser polarization is necessary for the two processes to coexist. The resultant sum-frequency beam is at a wavelength of 487 nm and is polarized along the fast axis of the crystal.

B. Sum-Frequency Optical Parametric Oscillator

Figure 1 shows our experimental setup, in which we use a ring cavity consisting of four mirrors that are high reflectors at the signal wavelength. Mirrors M1 and M2 are 100-mm radius-of-curvature concave, and M3 and M4 are flat. All cavity mirrors are high transmitters at the idler wavelength to ensure singly resonant operation. The 5-mm-long KTP crystal is placed at the intracavity focus between M1 and M2 with the fast axis parallel to the horizontal plane. The KTP crystal has antireflection coatings at the signal wavelength. We estimate that the cavity losses total 6% at the signal wavelength.

A mode-locked Ti:sapphire laser that has 170-fs-long pulses at a repetition rate of 76 MHz provides the pump beam at a wavelength of 827 nm. The output of the laser is *p* polarized, coinciding with the fast axis of the KTP crystal. A half-wave retarder (HWP) placed at the output of the laser provides adjustable polarization rotation for the pump beam. For a polarization rotation angle of α , a $\cos^2 \alpha$ fraction of the laser beam becomes the *p*-polarized OPO pump, whereas the remaining $\sin^2 \alpha$ fraction provides the *s*-polarized higher-frequency SFG input. These two polarization components are separated and recombined with the use of two polarizing beam splitters (PBS's) such that a variable group delay can be introduced between the pulses. This variable delay allows us

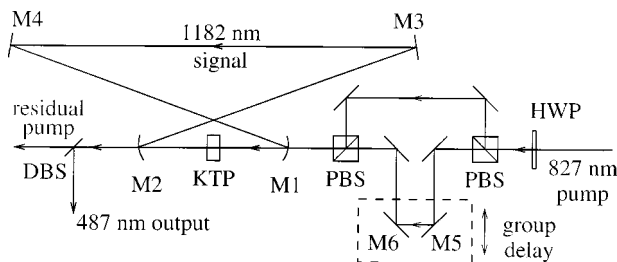


Fig. 1. Experimental setup for the SF-OPO. A mode-locked Ti:sapphire laser at a wavelength of 827 nm is used as the pump beam. Abbreviations are defined in text.

to compensate for the different group velocities that are experienced by the two polarization components inside the birefringent KTP crystal.

The recombined pump beam is focused with a lens (not shown) of 50-mm focal length and enters the cavity through M1, which has high-transmission coatings at the pump wavelength. The maximum pump power available to us in these experiments is 525 mW, measured before the focusing lens. The pump beam experiences a total loss of 1.9% in going through the focusing lens and M1, decreasing to 515 mW. The lowest-order transverse mode of the cavity has a 35- μm diameter (calculated), and the focused pump beam has a 48- μm diameter (measured) at the crystal. We synchronize the intracavity signal pulses with the pump pulses by adjusting the position of M3 with a piezoelectrically controlled mount. The blue sum-frequency beam emerges from the cavity through M2, which has 83% transmittance at this wavelength. This optic is also transparent at the pump and idler wavelengths. The diverging output beams are collimated with a lens (not shown) after M2. The sum-frequency beam is separated from the residual pump and the idler beams with a dichroic beam splitter (DBS). This beam experiences a total loss of 24% in going through the second KTP surface (4.3%), M2 (17%), the recollimating lens (2.5%), and the DBS (2.6%), because these surfaces were not coated specifically at the sum-frequency wavelength. The weak signal beam coming out through M3, owing to the slightly less than unity reflectance of this mirror, is used to monitor the beam profile of the intracavity signal field and to measure the intracavity signal power.

3. RESULTS AND DISCUSSION

In principle, there should be no phase-matched sum-frequency output when the polarization rotation angle is zero, because there is no *s*-polarized component at 827 nm. However, at this angle we observe a weak blue output beam (~ 4 mW at 515-mW pump power) that results from polarization impurity of the pump, from non-phase-matched SFG, or from both. As we increase polarization rotation angle α , a portion of the pump beam is coupled to *s* polarization and provides the higher-frequency SFG input. The resonant intracavity signal field is summed with the *s*-polarized pump component, resulting in a strong sum-frequency output beam at 487 nm and in decreased intracavity signal power. Hence the SFG process provides a nonlinear output coupling mechanism for the resonant signal field. Rotating the pump polarization also decreases the *p*-polarized pump power available for the parametric generation process, decreasing the intracavity signal. There is an optimum polarization rotation angle at which the blue output power is maximized. Further increase of the polarization angle decreases the output power until the SF-OPO falls below threshold.

In addition to the pump power and the polarization angle, the output sum-frequency power also depends on the group delay introduced between the *p*- and *s*-polarized components of the pump beam. We found that maximum conversion to the sum frequency is achieved when the *s*-polarized component leads the *p*-polarized component by 2 ps.

A. Conversion Efficiency

The power-conversion efficiency of the SF-OPO is the ratio of the output sum-frequency power to the input pump power. Additional linear losses incurred by the pump beam at the input and by the sum-frequency beam at the output are taken into account to reflect the true conversion efficiency. Figure 2 shows power-conversion efficiency as a function of polarization rotation angle at a pump power of 515 mW and group delay of 2 ps. The highest output power is 221 mW at a polarization angle of 36°, which corresponds to a power-conversion efficiency of 43%.

The SF-OPO falls below threshold at a polarization angle of 60°. The *p*-polarized component of the pump at this angle is 129 mW, which is much larger than the 25-mW threshold of the OPO at zero polarization angle. This result demonstrates that the parametric generation and SFG processes are strongly coupled to each other.

Because two photons at the pump wavelength are annihilated to create one sum-frequency photon, the photon-conversion efficiency of the SF-OPO is twice the ratio of the output sum-frequency photon flux to the input pump photon flux, so unity photon conversion efficiency represents total conversion. The maximum power-conversion efficiency shown in Fig. 2 corresponds to a photon-conversion efficiency of 50%.

Figure 3 shows the intracavity signal power and the depletion of the *p*- and *s*-polarized components of the pump as functions of the polarization angle. At 36°, where the conversion is highest, the intracavity signal power is only 3.7% of its value at 0°. Note that the depletion of the *s*-polarized component is very high and is almost constant for a wide range of polarization angle values starting from a few degrees all the way to 36°. Increasing the polarization angle above its optimum value results in a rapid decline, because then the intracavity signal power is no longer high enough to deplete the *s*-polarized pump component.

Figure 4 shows power-conversion efficiency as a function of pump power, where at each power level the polarization angle is optimized to yield maximum output power. The polarization rotation angle that maximizes

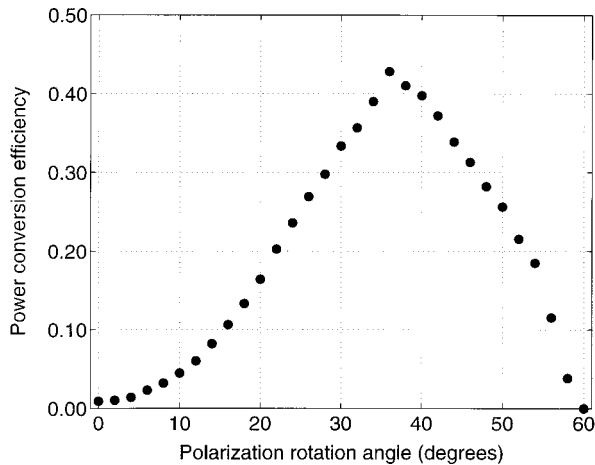


Fig. 2. Power-conversion efficiency as a function of polarization rotation angle. The pump power is 515 mW, and the group delay is 2 ps.

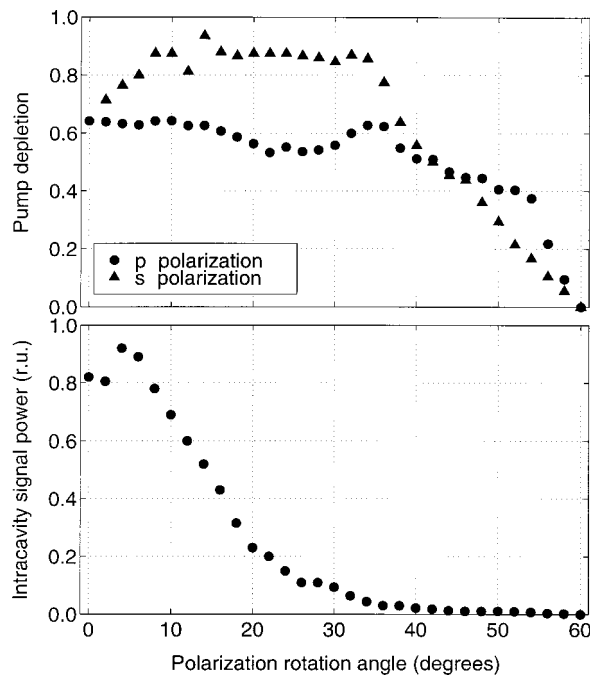


Fig. 3. Pump depletion for the *p*-polarized and the *s*-polarized components and the intracavity signal power (in relative units) as functions of polarization rotation angle. The pump power is 515 mW, and the group delay is 2 ps. r.u., Relative units.

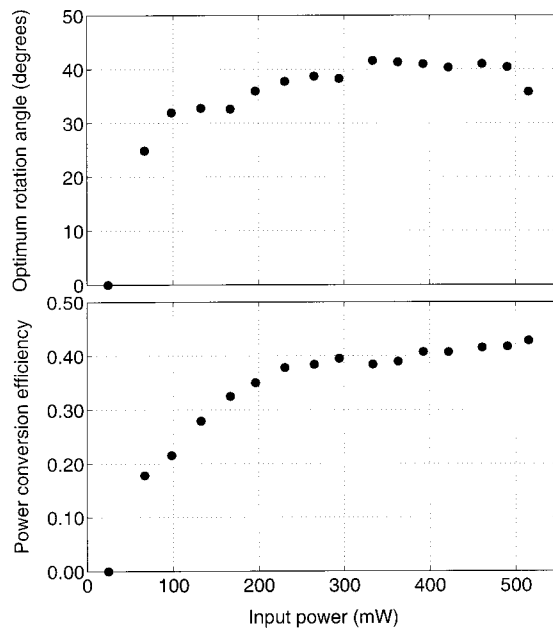


Fig. 4. Optimum polarization rotation angle and maximum power-conversion efficiency as functions of pump power.

the output power at each pump power level is also shown in the figure. Note that neither the conversion efficiency nor the optimum angle changes significantly for a wide range of the pump power.

B. Group Delay

The *p*- and *s*-polarized components of the pump pulse have different group velocities in the KTP crystal and get separated from each other as they propagate inside the

crystal. (The calculated¹³ group velocities of the interacting beams are 1.6631×10^8 m/s for the *p*-polarized pump, 1.5763×10^8 m/s for the *s*-polarized pump, 1.6896×10^8 m/s for the signal, 1.6094×10^8 m/s for the idler, and 1.5352×10^8 m/s for the sum frequency.) Inasmuch as the intracavity signal pulse is approximately synchronized with the *p*-polarized component (OPO pump), it falls out of synchronization with the *s*-polarized component (higher-frequency SFG input), thus reducing the efficiency of the SFG process. To compensate partially for this mismatch we adjust the group delay between the *p*- and *s*-polarized components before the pump beam enters the cavity by translating M5 and M6.

Figure 5 shows the power-conversion efficiency of the SF-OPO as a function of the group delay between the orthogonally polarized pump components at the entrance of the crystal. At each value of the delay, the polarization angle is adjusted to maximize the output power, while the input pump power is kept constant at 515 mW. With no group-delay adjustment setup, or with the delay adjusted to zero, we measure a maximum of 13% power-conversion efficiency at a polarization angle of 33° . Introducing a group delay of 2 ps increases the conversion efficiency by more than threefold. This delay is approximately equal to the group-velocity delay between the signal and the *s*-polarized pump component over 5 mm of KTP. For comparison, Fig. 5 shows a set of similar data, for a 1.5-mm-long KTP crystal instead. The power-conversion efficiency is 10.5%, when there is no delay. A 530-fs delay maximizes the power conversion-efficiency to 35%. Because this crystal is shorter than the 5-mm-long crystal, it requires a shorter group delay at the input for maximum conversion.

C. Tuning

It is possible to tune the SF-OPO by changing the phase-matching angle and the pump wavelength at the same time. Calculated tuning curves for the SF-OPO are shown in Fig. 6 together with experimental data points. By varying θ in the 90° – 60° range ($\phi = 0^\circ$) and the pump wavelength in the 827–887 nm range, one can generate an output wavelength of 487 to 554 nm. Tuning in the ϕ direction results in a narrower band compared with tuning in the θ direction; with ϕ varying from 0° to 30° ($\theta = 90^\circ$) and the pump wavelength varying from 827 to 817 nm, the output wavelength is tuned from 487 to 478 nm. Experimentally, we have demonstrated tunability in the 484–512 nm range, being limited by the bandwidth of the cavity mirrors and by reflection losses from the crystal surfaces.

We obtained the experimental data shown in Fig. 6 by maximizing the output power by adjusting the pump wavelength at each phase-matching angle. At a given phase-matching angle there is only one pair of signal and pump wavelengths that results in the simultaneous phase matching of the parametric generation and SFG processes. If the pump wavelength deviates from this value, the signal wavelength gets shifted, while the OPO stays phase matched; however, the SFG process is no longer phase matched. Therefore the output power of the SF-OPO is sensitive to the pump wavelength.

The relatively long crystal poses a number of minor inconveniences in tuning. Rotating the crystal not only changes the optical cavity length but also shifts the beams laterally. We can easily compensate for these effects by translating M3 and slightly realigning M2. The size of the transverse cavity mode and hence its overlap

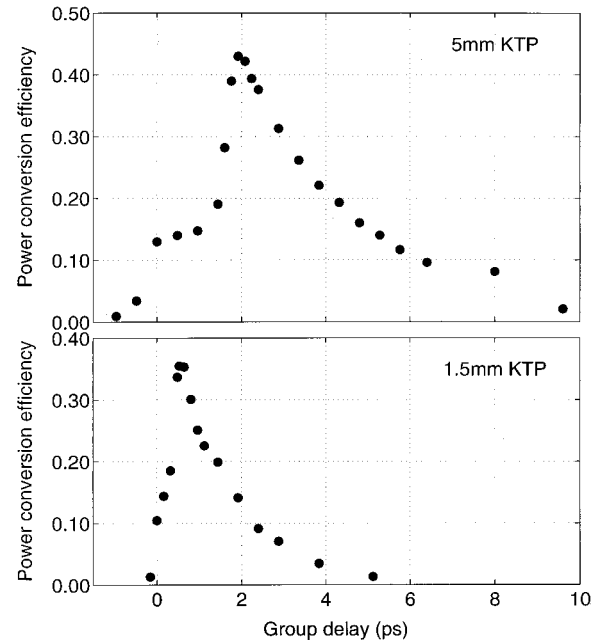


Fig. 5. Power-conversion efficiencies as functions of the group delay between the *p*- and the *s*-polarized pump components for 5- and 1.5-mm-long KTP crystals. The *p*-polarized component lags behind the *s*-polarized component for positive group-delay values.

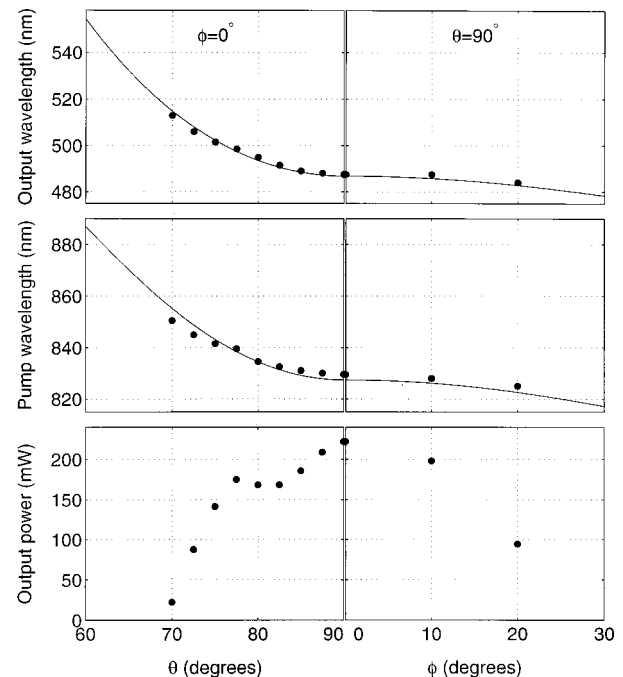


Fig. 6. Calculated tuning curves and measured values of output wavelength, pump wavelength, and output power across the tuning range for the SF-OPO. Angles are internal to the crystal. The filled circles represent experimental data points.

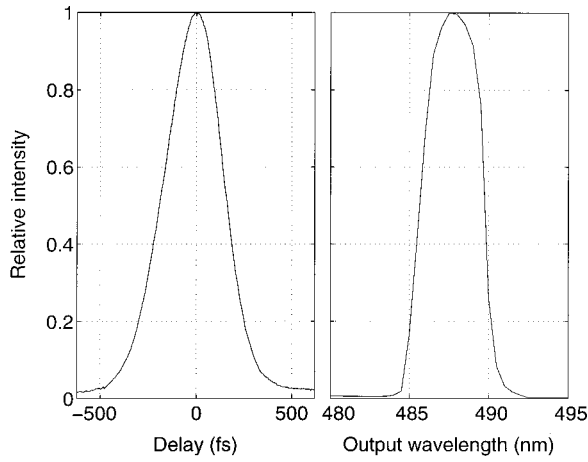


Fig. 7. Autocorrelation trace (left) and spectrum (right) of the sum-frequency output beam.

with the pump are influenced by the distance between M1 and M2, which also has to be readjusted after a rotation of the crystal.

D. Spectral and Temporal Characteristics

The spectrum and the autocorrelation of the sum-frequency output are shown in Fig. 7. The bandwidth of the spectrum is approximately 3.5 nm. The autocorrelation width of the sum-frequency pulses is measured to be 345 fs. When the output is deconvolved, assuming a secant hyperbolic (sech) shape, this corresponds to a pulse width of 225 fs, leading to a time–bandwidth product of unity. (For a transform-limited sech pulse the time–bandwidth product is 0.315.) The time–bandwidth product for the laser output is 0.45. This pulse broadening is due to group-velocity dispersion and the group-velocity mismatch between the *p*-polarized pump and the signal pulses in the KTP crystal. When we use a 1.5 mm-long KTP crystal, the pulse width of the sum-frequency beam reduces to 195 fs. This effect is due to reduced temporal overlap between the *s*-polarized pump and the signal.

To investigate the effects of group-velocity dispersion we constructed a linear (Fabry–Perot) cavity with intracavity dispersion-compensating prisms. Even though the presence of intracavity dispersion compensation reduced the bandwidth of the signal, it had little effect on the bandwidth or the pulse duration of the blue output beam.

4. PLANE-WAVE MODELING

Accurate modeling of the experiments reported in this paper requires one to include the effects of many experimental realities such as the temporal and transverse profiles of the pulses, group-velocity mismatch and dispersion, and self-phase modulation. We found that developing a plane-wave model that takes into account the temporal profile of the pulses and the group-velocity mismatch between these pulses gives us the most insight into the computation time. Our model does not take into account the Gaussian beam nature of the fields, chirped pulses, or group-velocity dispersion.

We begin with a set of plane-wave coupled-mode equations that govern the interaction of the pulses through the

nonlinear crystal that can be written as¹²

$$\frac{\partial a_i}{\partial Z} + \frac{1}{v_i} \frac{\partial a_i}{\partial t} = -j\kappa_a a_p a_s^*, \quad (1)$$

$$\frac{\partial a_s}{\partial Z} + \frac{1}{v_s} \frac{\partial a_s}{\partial t} = -j(\kappa_a a_p a_i^* + \kappa_b a_f a_r^*), \quad (2)$$

$$\frac{\partial a_p}{\partial Z} + \frac{1}{v_p} \frac{\partial a_p}{\partial t} = -j\kappa_a a_i a_s, \quad (3)$$

$$\frac{\partial a_r}{\partial Z} + \frac{1}{v_r} \frac{\partial a_r}{\partial t} = -j\kappa_b a_f a_s^*, \quad (4)$$

$$\frac{\partial a_f}{\partial Z} + \frac{1}{v_f} \frac{\partial a_f}{\partial t} = -j\kappa_b a_s a_r, \quad (5)$$

where a_m and v_m are normalized field amplitudes and group velocities for the idler (*i*), the signal (*s*), the pump (*p*), the rotated pump (*r*), and the sum-frequency (*f*) pulses, respectively. These normalized field amplitudes are related to the electric fields E_m through

$$a_m = (n_m c \epsilon_0 / 2 \hbar \omega_m)^{1/2} E_m, \quad m = i, s, p, r, f, \quad (6)$$

such that $|a_m|^2$ represents the photon flux density for each field at frequency ω_m . The nonlinear coupling coefficients are

$$\kappa_a = d_a \left(\frac{2\hbar}{c^3 \epsilon_0} \right)^{1/2} \left(\frac{\omega_i \omega_s \omega_p}{n_i n_s n_p} \right)^{1/2}, \quad (7)$$

$$\kappa_b = d_b \left(\frac{2\hbar}{c^3 \epsilon_0} \right)^{1/2} \left(\frac{\omega_s \omega_r \omega_f}{n_s n_r n_f} \right)^{1/2}, \quad (8)$$

where d_a and d_b are the effective nonlinear coefficients for the OPO and the SFG processes, respectively, and n_m are the refractive indices.

We used finite-differencing techniques to compute numerical solutions of Eqs. (1)–(5). In our calculations the pump field was modeled with a sech pulse shape. We started with a small-signal pulse that had the same sech shape as the pump to represent the parametric fluorescence from which the cavity oscillations build up. This signal pulse was iterated through the cavity several times, until a steady state was reached. At each round trip a fixed delay was introduced to the signal pulse to model the adjustment of the cavity length with M3. The group delay between the *p*- and the *s*-polarized components of the pump at the input was also adjustable.

We computed the photon-conversion efficiency for a series of cavity length (signal delay) values while keeping the polarization angle and the group delay constant. We found that, for a relevant range of polarization angle and group-delay values, the signal delay required for maximizing the conversion efficiency is in the 380–480-fs range. This conclusion is in agreement with the 472-fs group delay between the *p*-polarized pump and the signal in 5 mm of KTP. The maximum conversion efficiency that we obtained by varying the cavity length was taken to be the conversion efficiency at this polarization angle and group delay.

Next we set the group delay between the pump components to 2 ps and calculated the conversion efficiency for different values of the polarization angle. Figure 8

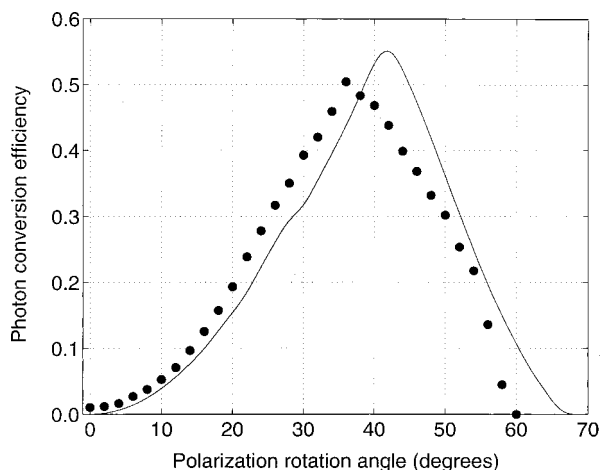


Fig. 8. Photon-conversion efficiency as a function of the polarization angle. Solid curve, theoretical plane-wave model; filled circles, experimental data points.

shows the results of this calculation together with experimental data points. We made no attempt to fit the predictions of the model to the data by adjusting any one of the physical parameters. The qualitative agreement of our model with the experimental results is highly satisfactory. The quantitative agreement for the peak photon conversion efficiency, the optimum polarization angle, and the threshold polarization angle is reasonably good.

At zero group delay we calculated the maximum photon conversion efficiency to be 22% at a polarization rotation angle of 30° . These results are also in reasonable agreement with those measured in our experiment.

Our model predicted a pulse width of 210 fs for the sum-frequency output, which is also in good agreement with the 225-fs value measured in the experiment. Because our model does not take group-velocity dispersion into account, this agreement suggests that group-velocity mismatch is the dominating factor in determining the pulse width.

5. CONCLUSIONS

In conclusion, we have demonstrated a sum-frequency-generating optical parametric oscillator for which both parametric generation and sum-frequency generation are phase matched simultaneously in a single nonlinear crystal. This SF-OPO provides upconversion of an ultrafast Ti:sapphire laser with 43% power-conversion efficiency (50% photon-conversion efficiency) in the two-step process from the pump to the signal and then to the sum frequency. To our knowledge, the value of this conversion efficiency is the highest ever reported for an upconversion OPO. In addition, we have developed a plane-wave model that is in very good agreement with our experiments.

The simultaneous phase matching of two different second-order nonlinear processes within the same crystal opens many frequency-conversion possibilities.¹⁴ Recent reports of second-harmonic generation^{15–18} and SFG^{11,16,19} within an OPO and within a cascaded OPO,²⁰ parametric amplification with SFG,²¹ and third-harmonic generation²² are some examples. Quasi-phase-matching

techniques will no doubt play a central role in realizing simultaneous phase matching.

ACKNOWLEDGMENT

This research was supported in part by the Turkish Scientific and Technical Research Council (Tubitak) under grants EEEAG-118 and 197E050.

O. Aytür can be reached at the address on the title page, by telephone at 90-312-290-2095, or by e-mail at aytur@ee.bilkent.edu.tr.

REFERENCES

1. R. L. Byer and A. Piskarskas, eds., feature on optical parametric oscillation and amplification, *J. Opt. Soc. Am. B* **10**, 1655–2243 (1993); W. R. Bosenberg and R. C. Eckardt, eds., feature on optical parametric devices, *J. Opt. Soc. Am. B* **12**, 2083–2320 (1995); C. L. Tang, W. R. Bosenberg, T. Ukachi, R. J. Lane, and L. K. Cheng, "Optical parametric oscillators," *Proc. IEEE* **80**, 365–374 (1992).
2. D. A. Roberts, "Simplified characterization of uniaxial and biaxial nonlinear optical crystals," *IEEE J. Quantum Electron.* **28**, 2057–2074 (1992).
3. L. E. Myers, R. C. Eckardt, M. M. Fejer, R. L. Byer, W. R. Bosenberg, and J. W. Pierce, "Quasi-phase-matched optical parametric oscillators in bulk periodically poled LiNbO₃," *J. Opt. Soc. Am. B* **12**, 2102–2116 (1995).
4. H. M. van Driel, "Synchronously pumped optical parametric oscillators," *Appl. Phys. B* **60**, 411–420 (1995).
5. D. C. Edelstein, E. S. Wachman, and C. L. Tang, "Broadly tunable high repetition rate femtosecond optical parametric oscillator," *Appl. Phys. Lett.* **54**, 1728–1730 (1989); W. S. Pelouch, P. E. Powers, and C. L. Tang, "Ti:sapphire pumped, high-repetition-rate femtosecond optical parametric oscillator," *Opt. Lett.* **17**, 1070–1072 (1992); Q. Fu, G. Mak, and H. M. van Driel, "High-power, 62-fs infrared optical parametric oscillator synchronously pumped by a 76-MHz Ti:sapphire laser," *Opt. Lett.* **17**, 1006–1008 (1992); G. Mak, Q. Fu, and H. M. van Driel, "Externally pumped high repetition rate femtosecond infrared optical parametric oscillator," *Appl. Phys. Lett.* **60**, 542–544 (1992); P. E. Powers, C. L. Tang, and L. K. Cheng, "High-repetition-rate femtosecond optical parametric oscillator based on CsTiOAsO₄," *Opt. Lett.* **19**, 37–39 (1994).
6. T. J. Driscoll, G. M. Gale, and F. Hache, "Ti:sapphire 2nd-harmonic-pumped visible range femtosecond optical parametric oscillator," *Opt. Commun.* **110**, 638–644 (1994).
7. A. Nebel, H. Frost, R. Beigang, and R. Wallenstein, "Visible femtosecond pulses by second harmonic generation of a cw mode-locked KTP optical parametric oscillator," *Appl. Phys. B* **60**, 453–458 (1995).
8. R. J. Ellingson and C. L. Tang, "High-power high-repetition-rate femtosecond pulses tunable in the visible," *Opt. Lett.* **18**, 438–440 (1993); D. T. Reid, M. Ebrahimzadeh, and W. Sibbett, "Efficient femtosecond pulse generation in the visible in a frequency-doubled optical parametric oscillator based on RbTiOAsO₄," *J. Opt. Soc. Am. B* **12**, 1157–1163 (1995).
9. E. C. Cheung, K. Koch, and G. T. Moore, "Frequency upconversion by phase-matched sum-frequency generation in an optical parametric oscillator," *Opt. Lett.* **19**, 1967–1969 (1994).
10. A. Shirakawa, H. W. Mao, and T. Kobayashi, "Highly efficient generation of blue–orange femtosecond pulses from intracavity-frequency-mixed optical parametric oscillator," *Opt. Commun.* **123**, 121–128 (1996).
11. K. G. Köprülü, T. Kartaloğlu, and O. Aytür, "Single-crystal sum-frequency generating optical parametric oscillator," in *Conference on Lasers and Electro-Optics*, Vol. 11 of 1997

- OSA Technical Digest Series (Optical Society of America, Washington, D.C., 1997), pp. 457–458.
12. O. Aytür and Y. Dikmelik, "Plane wave theory of self-doubling optical parametric oscillators," *IEEE J. Quantum Electron.* **34**, 447–458 (1998); Y. Dikmelik, G. Akgün, and O. Aytür, "Plane-wave dynamics of optical parametric oscillation with simultaneous sum-frequency generation," *IEEE J. Quantum Electron.* **35**, 897–912 (1999).
 13. K. Kato, "Parametric oscillation at 3.2 μm in KTP pumped at 1.064 μm ," *IEEE J. Quantum Electron.* **27**, 1137–1140 (1991).
 14. R. A. Andrews, H. Rabin, and C. L. Tang, "Coupled parametric downconversion and upconversion with simultaneous phase matching," *Phys. Rev. Lett.* **25**, 605–608 (1970).
 15. T. Kartaloğlu, K. G. Köprülü, and O. Aytür, "Phase-matched self-doubling optical parametric oscillator," *Opt. Lett.* **22**, 280–282 (1997).
 16. K. C. Burr, C. L. Tang, M. A. Arbore, and M. M. Fejer, "Broadly tunable mid-infrared femtosecond optical parametric oscillator using all-solid-state-pumped periodically poled lithium niobate," *Opt. Lett.* **22**, 1458–1460 (1997).
 17. C. McGowan, D. T. Reid, Z. E. Penman, M. Ebrahimzadeh, W. Sibbett, and D. H. Jundt, "Femtosecond optical parametric oscillator based on periodically poled lithium niobate," *J. Opt. Soc. Am. B* **15**, 694–701 (1998).
 18. D. T. Reid, G. T. Kennedy, A. Miller, W. Sibbett, and M. Ebrahimzadeh, "Widely tunable, near- to mid-infrared femtosecond and picosecond optical parametric oscillators using periodically poled LiNbO₃ and RbTiOAsO₄," *IEEE J. Sel. Top. Quantum Electron.* **4**, 238–248 (1998).
 19. S. D. Butterworth, P. G. R. Smith, and D. C. Hanna, "Picosecond Ti:sapphire-pumped optical parametric oscillator based on periodically poled LiNbO₃," *Opt. Lett.* **22**, 618–620 (1997).
 20. M. Vaidyanathan, R. C. Eckardt, V. Dominic, L. E. Myers, and T. P. Grayson, "Cascaded optical parametric oscillations," *Opt. Express* **1**, 49–53 (1997), <http://epubs.osa.org/opticsexpress>.
 21. V. Petrov and F. Noack, "Frequency upconversion of tunable femtosecond pulses by parametric amplification and sum-frequency generation in a single nonlinear crystal," *Opt. Lett.* **20**, 2171–2173 (1995).
 22. O. Pfister, J. S. Wells, L. Hollberg, L. Zink, D. A. van Baak, M. D. Levenson, and W. R. Bosenberg, "Continuous-wave frequency tripling and quadrupling by simultaneous three-wave mixings in periodically poled crystals: application to a two-step 1.19–10.71- μm frequency bridge," *Opt. Lett.* **22**, 1211–1213 (1997).